Published OnlineFirst May 23, 2017; DOI: 10.1158/1541-7786.MCR-17-0105

Signal Transduction

Molecular Cancer Research

MELK and EZH2 Cooperate to Regulate Medulloblastoma Cancer Stem-like Cell Proliferation and Differentiation

Hailong Liu[1], Qianwen Sun[2], Youliang Sun[3], Junping Zhang[1], Hongyu Yuan[4], Shuhuan Pang[5], Xueling Qi[6], Haoran Wang[1], Mingshan Zhang[1], Hongwei Zhang[1], Chunjiang Yu[1], and Chunyu Gu[1]

Abstract

Medulloblastoma is the most common malignant brain tumor in children. Although accumulated research has suggested that cancer stem-like cells play a key role in medulloblastoma tumorigenesis, the specific molecular mechanism regarding proliferation remains elusive. Here, we reported more abundant expression of maternal embryonic leucine-zipper kinase (MELK) and enhancer of zeste homolog 2 (EZH2) in medulloblastoma stem-like cells than in neural stem cells and the interaction between the two proteins could mediate the self-renewal of sonic hedgehog subtype medulloblastoma. In human medulloblastoma, extensive nodularity and large-cell/anaplastic subgroups differed according to the staining levels of MELK and EZH2 from the other two subgroups. The proportion of MELK- or EZH2-positive staining status could be considered as a potential indicator for survival. Mechanistically, MELK bound to and phosphorylated EZH2, and its methylation was induced by EZH2 in medulloblastoma, which could regulate the proliferation of cancer stem-like cells. In xenografts, loss of MELK or EZH2 attenuated medulloblastoma stem-like cell-derived tumor growth and promoted differentiation. These findings indicate that MELK-induced phosphorylation and EZH2-mediated methylation in MELK/EZH2 pathway are essential for medulloblastoma stem-like cell-derived tumor proliferation, thereby identifying a potential therapeutic strategy for these patients.

Implications: This study demonstrates that the interaction occurring between MELK and EZH2 promotes self-proliferation and stemness, thus representing an attractive therapeutic target and potential candidate for diagnosis of medulloblastoma. *Mol Cancer Res; 1–12. ©2017 AACR.*

Introduction

Medulloblastoma is the most common pediatric malignant brain tumor, accounting for about 20% of children with intracranial tumors (1, 2). According to the 2016 WHO classification of CNS tumor (3), medulloblastoma comprises four histologic subgroups, including desmoplastic/nodular, classic, extensive nodularity, and large-cell/anaplastic, and also four molecular subtypes, including SHH, WNT, Group 3 and Group 4. Mainstream treatment for medulloblastoma focuses on the surgical resection with maximal security followed by radiation and chemotherapy. Despite the significant progression in current therapeutic strategies, the 5-year survival rate in high-risk group is only about 40% (4, 5), and about half of patients suffer from metastasizing along the leptomeninges via CSF (6). Patients receiving radio- or chemotherapy have to bear the life-long physiologic and psychologic side effects. Therefore, improved prevention and treatment of this disease will require deeper understanding of the cellular and molecular basis of medulloblastoma.

Cancer stem-like cells (CSC) have been regarded as being involved in tumorous proliferation, invasion, recurrence, and chemoradioresistance, which creates a new concept of tumorigenicity and progression (7, 8). It has been hypothesized that medulloblastoma may also derive from this stem-like population, which contributes to self-renewal, relapse, and resistance to chemoradiotherapy (9, 10). Then, the treatment failure is due to the current therapy, which only impacts the bulk tumor but does not target the CSCs. It is essential to develop a new therapeutic strategy to solve this problem with the goal of improving patients' survival.

The serine/threonine kinase, maternal embryonic leucine-zipper kinase (MELK), is categorized to the snf1/AMPK family (11) and has been reported to enrich in a wide range of cancers (12–17), especially in glioblastoma multiforme (GBM) previously described by Gu and colleagues (Supplementary Fig. S1A; ref. 18). Some specific pathways, such as C-JUN/MELK and MELK/PRC1, are activated in GBM for the survival of CSCs (18, 19). In the previous work (18), GBM CSCs (GSC) were identified to depend on JNK-driven MELK/c-JUN signaling to

[1]Department of Neurosurgery, Sanbo Brain Hospital Capital Medical University, Beijing, P.R. China. [2]Department of Neurology, Qilu Hospital Shandong University, Jinan, P.R. China. [3]School of Basic Medical Science, Capital Medical University, Beijing, P.R. China. [4]State Key Laboratory of Molecular Oncology, National Cancer Center/Cancer Hospital, Chinese Academy of Medical Sciences and Peking Union Medical College, Beijing, P.R. China. [5]Temple University, Philadelphia, Pennsylvania. [6]Department of Pathology, Sanbo Brain Hospital Capital Medical University, Beijing, P.R. China.

Note: Supplementary data for this article are available at Molecular Cancer Research Online (http://mcr.aacrjournals.org/).

Corresponding Authors: Chunyu Gu, Department of Neurosurgery, Sanbo Brain Hospital Capital Medical University, No. 50 Yi-ke-song Road, Xiangshan Ave, Beijing 100093, P.R. China. Phone: 8610-6285-6704; Fax: 8610-6285-6902; E-mail: neurosurgery2@163.com; and Chunjiang Yu, cjyu1955@sina.com

doi: 10.1158/1541-7786.MCR-17-0105

Published OnlineFirst May 23, 2017; DOI: 10.1158/1541-7786.MCR-17-0105

maintain the proliferation and facilitate tumor radioresistance in a p53-dependent manner. Nevertheless, it is noteworthy that only some limited available information about the expression of MELK can be checked in medulloblastoma research field (14, 19), and the functional mechanisms or interaction with other main proteins still remain elusive. Furthermore, therapies targeting this potential molecular mechanism have not been developed.

Enhancer of zeste homolog 2 (EZH2), one member of the complex of c-Myc/HBXIP/Hotair/LSD1 (20), is also the core component of polycomb repressive complex 2 (PRC2; refs. 21–23), which makes sense in histone epigenetic methylation as one assembly of the polycomb group (24–27). According to the existing data, high expression of EZH2 has been detected in a broad spectrum of cancers, including medulloblastoma (Supplementary Fig. S1B; refs. 28–32). Recent research indicates that EZH2 as the transcriptional silencer produces the oncogenic effects for promoting neoplastic proliferation, maintaining the stem-like features, and inhibiting differentiation (31, 33). In medulloblastoma, EZH2 can regulate the expression of DAB2IP (29) and mediate aberrant methylation of H3K27 (34). Then, there exists a challenging puzzle whether it can induce the methylation of MELK in medulloblastoma.

Recent studies (35, 36) show that MELK and EZH2 colocate and abundantly express in the GSCs nuclei, and a significant positive correlation exists between the two proteins in human gliomas. These backgrounds throw light on the subsequent research about the interaction between MELK and EZH2 in medulloblastoma to present the evidence supporting a novel application for targeted therapy. In the current study, we investigated the differential expression of MELK and EZH2 in four histologic subgroups of medulloblastoma and analyzed the association with prognosis. Moreover, we detected the MELK-mediated phosphorylation of EZH2 and the EZH2-induced methylation of MELK, as well as compared the levels of two proteins in neural stem cells (NSC) and CSCs. Finally, we inhibited MELK and EZH2 by RNAi and inhibitor techniques to verify the critical role of MELK/EZH2 pathway in regulating the proliferation of SHH subgroup medulloblastoma CSCs (MBSC). To the best of our knowledge, it is the first novel study to demonstrate the crucial role of interaction between MELK and EZH2 in maintaining medulloblastoma proliferation. This study will further provide the framework to develop the promising therapeutic approaches for medulloblastoma, through targeting the MBSC stem features.

Materials and Methods

Samples and cells

The medulloblastoma specimens were obtained from 88 patients undergoing craniotomy at the Department of Neurosurgery in Sanbo Brain Hospital, Capital Medical University (Beijing, P.R. China) from September 2010 to February 2016. None of the tumors had received chemo- and radiotherapy before surgery. All the samples were reviewed and diagnosed by two experienced neuropathologists. All tissues were collected during operation, and then were frozen and stored in liquid nitrogen. Patient and tumor characteristics are shown in Table 1, and survival analysis was based on this cohort of 88 cases. All procedures were approved by the Research Ethics Committee of our institute, and written informed consent was obtained from each patient included in the study.

Table 1. Characteristics of patients with medulloblastoma (88 cases)

Items	*N* (%)	OR
Gender		0.67
Male	46 (52.27)	
Female	42 (47.73)	
Age (y)		1.13
<3	13 (14.78)	
3–16	51 (57.95)	
>16	24 (27.27)	
Prognosis		0.72
Alive	39 (44.32)	
Dead	49 (55.68)	
Risk stage		1.56
M0	31 (35.23)	
M1	8 (9.09)	
M2	49 (55.68)	
MELK		2.01
<49.0%	43 (48.86)	
>50.0%	45 (51.14)	
EZH2		1.05
<49.0%	47 (53.41)	
>50.0%	41 (46.59)	
Ki-67		1.96
<30.0%	25 (28.41)	
30.0–60.0%	44 (50.00)	
>60.0%	19 (21.59)	
Pathology		1.32
Desmoplastic/nodular MB	12 (13.64)	
Classic MB	47 (53.41)	
MB with extensive nodularity	7 (7.95)	
Large-cell/anaplastic MB	22 (25.00)	

Abbreviation: MB, medulloblastoma.

Human medulloblastoma Daoy cell line was obtained from National Infrastructure of Cell Line Resource in Peking Union Medical College (Beijing, P.R. China) in June 2013. The cell line in C4 passage before thawing was confirmed free of mycoplasma contamination by PCR, and the species origin was also confirmed by PCR, with the results being viewed on the official website (http://cellresource.cn). The identity was authenticated with STR profiling (FBI, CODIS), and the tests were performed before cells were cryopreserved or one of the vials from a lot was taken out for examination. Primary human MB25550 cells were established from fresh specimens in our institute as described previously (Supplementary Fig. S2; ref. 38). All the tumor cells were maintained in DMEM supplemented with 10% FBS at 37°C in a humidified 5% CO_2 incubator.

Main reagents

The MELK inhibitor, OTSSP167, and EZH2 inhibitor, DZNep, were purchased from Sigma. The following agents were purchased from Gibco: DMEM/F12 medium, Neurobasal medium, B27, basic FGF (bFGF), EGF, and L-glutamine.

Tissue culture

Chippy human medulloblastoma tissues were digested with 0.25% trypsin and resuspended at 1×10^7 cells/mL in DMEM/F12 medium with B27 (2%), bFGF (20 ng/mL), EGF (50 ng/mL), L-glutamine (1%), and penicillin/streptomycin (1%) to isolate the CSCs. After being dissociated into single cells, the abovementioned cells were cultured in DMEM with 10% FBS to differentiate tumor cells. Fractions of fetal or adult mouse cortex were digested with 0.25% trypsin and resuspended at 1×10^7 cells/mL in Neurobasal medium with B27 (2%), L-glutamine (1%), and penicillin/streptomycin (1%) to isolate

Published OnlineFirst May 23, 2017; DOI: 10.1158/1541-7786.MCR-17-0105

the neurons (binding part) and gliocytes (suspended part). The suspended gliocytes were collected and cultured in DMEM with 10% FBS. When small hippocampus tissues were digested and dissociated into single cells, FACS was performed with the CD133 antibody (Abcam) for sorting of the NSCs, and then, the obtained cells were cultured in Neurobasal medium containing B27 (2%), bFGF (20 ng/mL), EGF (50 ng/mL), L-glutamine (1%), and penicillin/streptomycin (1%).

IHC and immunofluorescence staining

All the 5-μm thick sections were prepared from paraffin-embedded tissues. In brief, sections were stained with the anti-MELK, EZH2, Nestin, or NeuN antibodies (1:100) at 4°C overnight. Then, the sections were washed and incubated using secondary antibodies for 1 hour. Two experienced pathologists in our institute estimated the number of positive staining cells by counting 500 nuclei in four high magnification fields (400×) randomly as the percentage. Histologic subtypes were also achieved by two pathologists in our institute.

Tissue sections, neurospheres, or dissociated MBSCs were incubated with blocking liquid for 1 hour and subsequently incubated with anti-MELK, EZH2, CD133, Nestin, GFAP, or Ki-67 antibodies (1:200) overnight at 4°C and FITC secondary antibody at room temperature for 1 hour.

RNA extraction and RT-PCR

RNA was isolated from Daoy and MB25550 tumor cells and MBSCs using TRIzol reagent according to the manufacturer's instructions (Invitrogen). cDNA was synthesized by using iScript reverse transcription reagent from 2 μg of total RNA. The relative levels of mRNA were determined by using SYBR Green on the Mx3000P QPCR system and normalized for the expression of GAPDH mRNA. The following sequences were used for the primers, MELK: 5′-CACCGCAGCAGCAGGCAGAC-3′, 3′-GGGTTGGTGAGGCGGGTATTTC-5′; EZH2: 5′-CCCTTCTCAGATTTCTTCCCA-3′, 3′-GAGGTGACGGAAGACTCAGG-5′.

Cell and tissue lysis

Cells and tissues were lysed by using ice-cold buffer with 0.1% Triton X-100 and 20 mmol/L Tris-HCl (pH = 7.4) containing protease inhibitor cocktail. Protein concentration was measured by bicinchoninic acid assay according to the manufacturer's protocol (Invitrogen).

Western blot analysis

The whole protein (50 μg) was separated by 10% SDS-PAGE gel and then transferred to the PVDF membranes. The membranes were subsequently incubated with anti-MELK, EZH2, Nestin, NeuN, β-actin antibodies (Sigma) and anti-SUV391H1, p-KMT6/EZH2, and H3K27me3 antibodies (Abcam) overnight at 4°C. Secondary antibodies were used to probe the membranes for 1 hour at room temperature. All primary antibodies were diluted at 1:500 expect for β-actin (at 1:3,000).

Coimmunoprecipitation

Anti-MELK and anti-EZH2 antibodies or anti-SUV391H1 and anti-p-KMT6/EZH2 antibodies cross-linked with protein A/G beads were incubated with 500 μg of lysates from tumor cells and MBSCs overnight at 4°C, respectively. Then, protein was eluted from beads and added into the 10% SDS-PAGE gel for electrophoresis. Immunoblotting for the indicated antibodies was performed.

MELK and EZH2 knockdown by siRNA and shRNA

siRNA was synthesized using the Silencer siRNA Construction Kit (Applied Biosystems/Ambion) as previously described according to the manufacturer's instructions (37). Lentiviral vectors were produced by transfecting human embryonic kidney (HEK) 293T cells with the MELK or EZH2 shRNA construct together with the packaging agents pMD2.G and psPAX2 using Lipofectamine 2000 (Invitrogen). After removal of cell debris with filter, the supernatant containing lentivirus was used to infect MBSCs. The sequence targeting MELK and EZH2 were: MELK sense, AATACCCACATCGGTTTCCTGTCTC, antisense, AAAAACCCGATGTGGTGGGTACCTGTCTC; EZH2 sense, CCGGGCTAGGTTAATTGGGACCAAA, antisense, CTCGAGTTTGGTCCCAATTAACCT.

Cell proliferation and colony formation assay

Dissociated MB25550 CSCs transfected with siMELK, siEZH2, and nontarget siRNA were seeded in 60-mm dishes coated with gelatin and cultured in DMEM/F12 without FBS. Dissociated Daoy CSCs were seeded in 60-mm dishes coated with gelatin and cultured in the presence of OTSSP167, DZNep, and PBS. After 10 days, the cells were immersed into 4% paraformaldehyde and 0.1% crystal violet.

Transwell assay

Migration assay was performed using the Transwell chambers. Briefly, Daoy cells differentiated from the MELK-, EZH2-, and nontarget deficient MBSCs (1×10^3 in 100 μL) were added into the upper chambers, while the lower chambers were filled with 500 μL of DMEM with 10% FBS. After 8 hours, the filters were then fixed and stained with 0.1% crystal violet, then counted.

Transplantation and drug administration

All animal experiments were performed in accordance with national guidelines at Capital Medical University (Beijing, P.R. China) and approved by our institutional ethics committee. Dissociated Daoy or MB25550 CSCs infected with shMELK, shEZH2, and nontarget shRNA (1×10^7 cells in 100 μL) were subcutaneously injected into the left (experimental) and right (control) flank of 6- to 8-week-old male Bal-B/C nude mice ($n = 6$/group). Tumor volumes were measured every 3 days and calculated according to the following formula: $V\ (mm^3) = 1/2\ (L \times W^2)$. After 1 month, the mice were sacrificed and tumors sections were stained with anti-Ki-67 antibody.

The above infected MB25550 CSCs (5×10^6 cells in 5 μL) were used for the intracranial injection into the right hemisphere by using a mouse stereotaxic apparatus as described previously (38). MicroMRI scanning and PET/CT were performed (on the 28th day) to investigate tumor growth and metastasis. Survival was defined as the time from transplantation until death. Tumor sections were stained with anti-Ki-67, Nestin, and NeuN antibodies.

The OTSSP167 and DZNep were utilized as the MELK and EZH2 inhibitors to complement these findings, which have been involved in a great deal of research (39–41). On the 5th day after intracranial transplantation of dissociated MB25550 CSCs, engraftments were confirmed with microMRI scanning, and mice with equivalent volumes were randomized into three groups for intraperitoneal treatment: OTSSP167 (20 mg/kg), DZNep (20 mg/kg), and control ($n = 6$/group). Tumor growth was measured by microMRI scanning on the 28th day, and the adverse actions of inhibitors were reflected by mice weight. Until tumor-associated

Published OnlineFirst May 23, 2017; DOI: 10.1158/1541-7786.MCR-17-0105

morbidity, immunostaining for Ki-67 in tumor sections was handled as above.

Public gene data

The data of MELK and EZH2 profiles in The Cancer Genome Atlas (TCGA) database are available for analysis on the cBioPortal website (http://www.cbioportal.org). MELK and EZH2 expression data in molecular subgroups of medulloblastoma were checked in GSE50765 dataset from R2 database (https://hgserver1.amc.nl).

Statistical analysis

Statistical data handling was performed using SPSS 18.0 and GraphPad Prism 7.0 software, and values were shown as mean ± SD and error bars represented as SEM. Statistical significance between two groups was determined by *t* test, and comparison of mean values between multiple groups was evaluated by one-way ANOVA. Correlations of staining indexes were analyzed by the Pearson test. Overall survival (OS) was assessed using Kaplan–Meier method, and the log-rank test was adopted for significance of differences between survival curves. Variable prognostic factors were analyzed by Cox proportional model. For all statistical methods, $P < 0.05$ was considered statistically significant.

Results

Overexpression of MELK and EZH2 correlated with prognosis of medulloblastoma patients

To identify the expression of MELK and EZH2 in medulloblastoma, 94 cases in total were collected in the current research, including desmoplastic/nodular medulloblastoma ($n = 12$), classic medulloblastoma ($n = 47$), medulloblastoma with extensive nodularity ($n = 7$), large-cell/anaplastic medulloblastoma

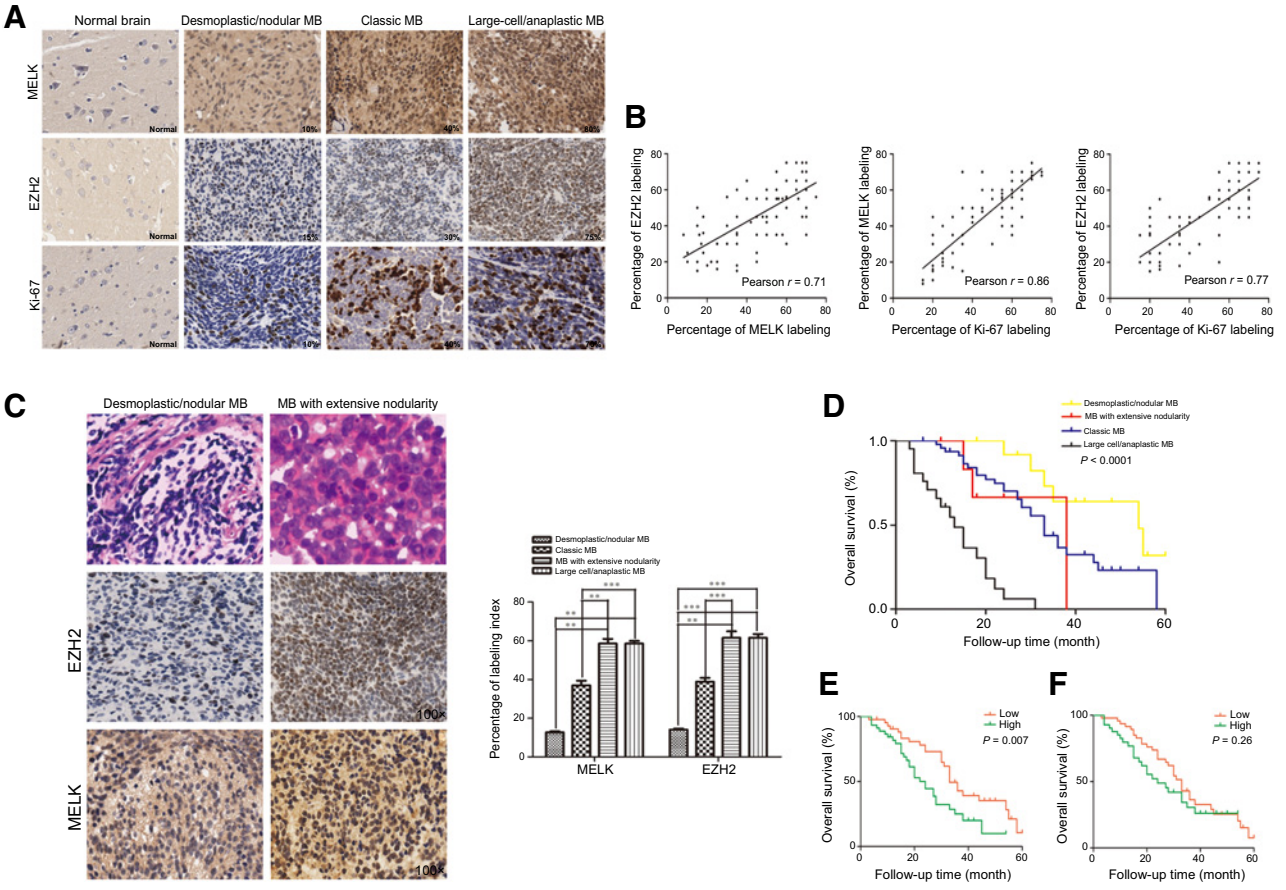

Figure 1.

MELK and EZH2 proteins were abundantly enriched in medulloblastoma (MB) specimens. **A,** Representative IHC images in low magnification fields (100×) showed that MELK, EZH2, and Ki-67 highly expressed in human medulloblastoma tissues compared with normal brain, and the staining levels could be ranked in three grades. **B,** MELK or EZH2 and Ki-67 expression in 88 specimens were compared for their correlation. The Pearson coefficients were 0.71, 0.86, and 0.77, respectively. **C,** Left, representative images of MELK and EZH2 expression in desmoplastic/nodular and extensive nodularity subtypes of medulloblastoma in low magnification fields (100×). The first line showed the morphology in high magnification fields (H&E, 200×). Right, statistical graph showed that staining levels of MELK and EZH2 in large-cell/anaplastic medulloblastoma were significantly higher than those in other subgroups ($P < 0.01$, $P < 0.0001$). **D,** The association between OS and histologic subtypes was evaluated by Kaplan–Meier analysis, indicating that patients with desmoplastic/nodular and classic subtypes had more OS benefit ($P < 0.0001$). **E** and **F,** Patients were divided into two groups according to the MELK (**E**) or EZH2 (**F**) expression levels (low, percentage of positively stained cells was lower to 49.0%; high, percentage of positively stained cells was more than 50.0%), and the postsurgical survival rate was evaluated by Kaplan–Meier analysis. There was a significant difference between the high and low MELK staining group, but not in EZH2 expression ($P < 0.01$, $P = 0.26$).

Published OnlineFirst May 23, 2017; DOI: 10.1158/1541-7786.MCR-17-0105

($n = 22$), and normal cerebra ($n = 6$), to assess the MELK, EZH2, and Ki-67 staining levels by IHC (Table 1). Figure 1A showed that MELK and EZH2 abundantly expressed in nuclei of medulloblastoma cells compared with the normal cerebra, and the staining levels could be ranked in three grades, shown as the weak positive (<30.0%), median positive (30.0%–60.0%), and strong positive (>60.0%). We analyzed the correlation between MELK and EZH2 by Pearson analysis, indicating that a positive tendency was present between the two proteins (Fig. 1B). The similar correlation could also be obtained in the SHH-MB dataset (Supplementary Fig. S1C) from R2 Database. Then, the findings were also in parallel with the correlation in glioma (Supplementary Fig. S1D) according to the TCGA database (42). In addition, at protein levels, the statistically significant association of MELK or EZH2 with Ki-67 supported their strong dependability on proliferation (Fig. 1B). Then, we checked the differential expression in histologic subgroups, showing that both proteins were substantially higher in extensive nodularity and large-cell/anaplastic medulloblastoma than the normal and other two subgroups (Fig. 1C).

The clinical characteristics utilized for survival analysis in this cohort of cases are summarized in Table 2. Among the 88 cases, the median follow-up time was 36.3 months (range, 3.0–65.0 months); 39 patients (44.32%) were still alive, and there were 49 deaths (55.68%) due to medulloblastoma during the follow-up periods. The analysis of OS using variable histologic subgroups was generated by Kaplan–Meier method, conferring that patients with desmoplastic/nodular and classic characteristics showed more survival benefit (Fig. 1D). To analyze the prognostic impacts of both proteins, 88 tumors were divided into two groups based on the average of MELK or EZH2 immunostaining intensities. Patients with higher MELK levels had poorer postoperative survival, but a similar result was not obtained in EZH2 (Fig. 1E and F). However, the assessment of some possible clinicopathologic factors by Cox proportional model and the OR data by logistic analysis showed that not only MELK, but also EZH2 could be taken into account as the prognostic indicator (Table 1; Supplementary Table S1). Taken together, these data ruled out that both MELK and EZH2 contributed to predicting histologic diagnosis and postsurgical survival of medulloblastoma patients.

MELK and EZH2 protein colocated in MBSCs

Using a stringent dilution cloning formation method, Daoy and MB25550 CSCs were isolated from Daoy cell line and primary MB25550 cells. To identify the immunophenotype of CSCs, staining for stem cell marker CD133 was performed, showing notable expression in the MBSCs (Fig. 2A). To confirm the interaction between MELK and EZH2 in MBSCs, coexpression and localization were investigated by immunofluorescence. As shown in Fig. 2B and C, MELK and EZH2 positively expressed in the dissociate MBSCs and neurospheres, which were colabeled with the other stem cell marker, Nestin. We further performed confocal immunofluorescence staining in the single CSC to show MELK and EZH2 colocated in the nuclei (Fig. 2D). The upregulated levels of MELK and EZH2 were observed when they were examined in the SHH-MB dataset (GSE50765; Supplementary Fig. S3A). Similarly, the expression was also confirmed in medulloblastoma tissues developed from the *Ptch1* heterozygous mice by viewing the high magnification fields (Fig. 2E; Supplementary Fig. S3B). Immunostaining for MELK or EZH2 and GFAP in human medulloblastoma tissues (Supplementary Fig. S3C) and tumor tissues of $Ptc^{+/-}$ mouse model (Fig. 2F) showed that both of the two proteins highly expressed and astrocytes were activated, but not in normal cerebellum (Supplementary Fig. S3C and S3D). To corroborate these staining findings with the cancerous stem features in MBSCs, we observed markedly elevated relative mRNA levels of *melk* and *ezh2* in MBSCs, but little differential expression in the non-CSCs (Fig. 2G; Supplementary Fig. S3E). Immunoblotting of the cell lysates confirmed a stronger expression of MELK and EZH2 in tumorigenic CSCs from Daoy and MB25550, compared with their sister cultures in the medium containing FBS (Fig. 2H). Thus, these data suggested that MELK and EZH2 colocalized in MBSCs were required to maintain the stemness.

Table 2. Characteristics of medulloblastoma patients used for survival analysis (88 cases)

Items	Low MELK (<49.0%)	High MELK (>50.0%)	Low EZH2 (<49.0%)	High EZH2 (>50.0%)
Total of cases	43 (48.86)	45 (51.14)	48 (54.55)	40 (45.45)
Gender				
Male	27 (62.79)	22 (48.89)	31 (64.58)	18 (45.00)
Female	16 (37.21)	23 (51.11)	17 (35.42)	22 (55.00)
Age (y)				
<3	4 (9.30)	5 (11.11)	5 (10.42)	4 (10.00)
3–16	27 (62.79)	24 (53.33)	31 (64.58)	20 (50.00)
>16	12 (27.91)	16 (35.56)	12 (25.00)	16 (40.00)
Risk stage				
M0	17 (39.53)	14 (31.11)	19 (39.58)	12 (30.00)
M1	4 (9.30)	4 (8.89)	3 (6.25)	5 (12.50)
M2	22 (51.16)	27 (60.00)	26 (54.17)	23 (57.50)
Ki-67				
<30.0%	21 (48.84)	0 (0)	19 (39.58)	2 (5.00)
30.0%–60.0%	19 (44.19)	20 (44.44)	27 (56.25)	12 (30.00)
>60.0%	3 (6.98)	25 (55.56)	2 (4.17)	26 (65.00)
Pathology				
Desmoplastic/nodular MB	8 (18.60)	4 (8.89)	9 (18.75)	3 (7.50)
Classic MB	33 (76.74)	15 (33.33)	36 (75.00)	12 (30.00)
MB with extensive nodularity	0 (0)	7 (15.56)	0 (0)	7 (17.50)
Large-cell/anaplastic MB	2 (4.65)	19 (42.22)	3 (6.25)	18 (45.00)

NOTE: Data are presented as number (percentage).
Abbreviation: MB, medulloblastoma.

Published OnlineFirst May 23, 2017; DOI: 10.1158/1541-7786.MCR-17-0105

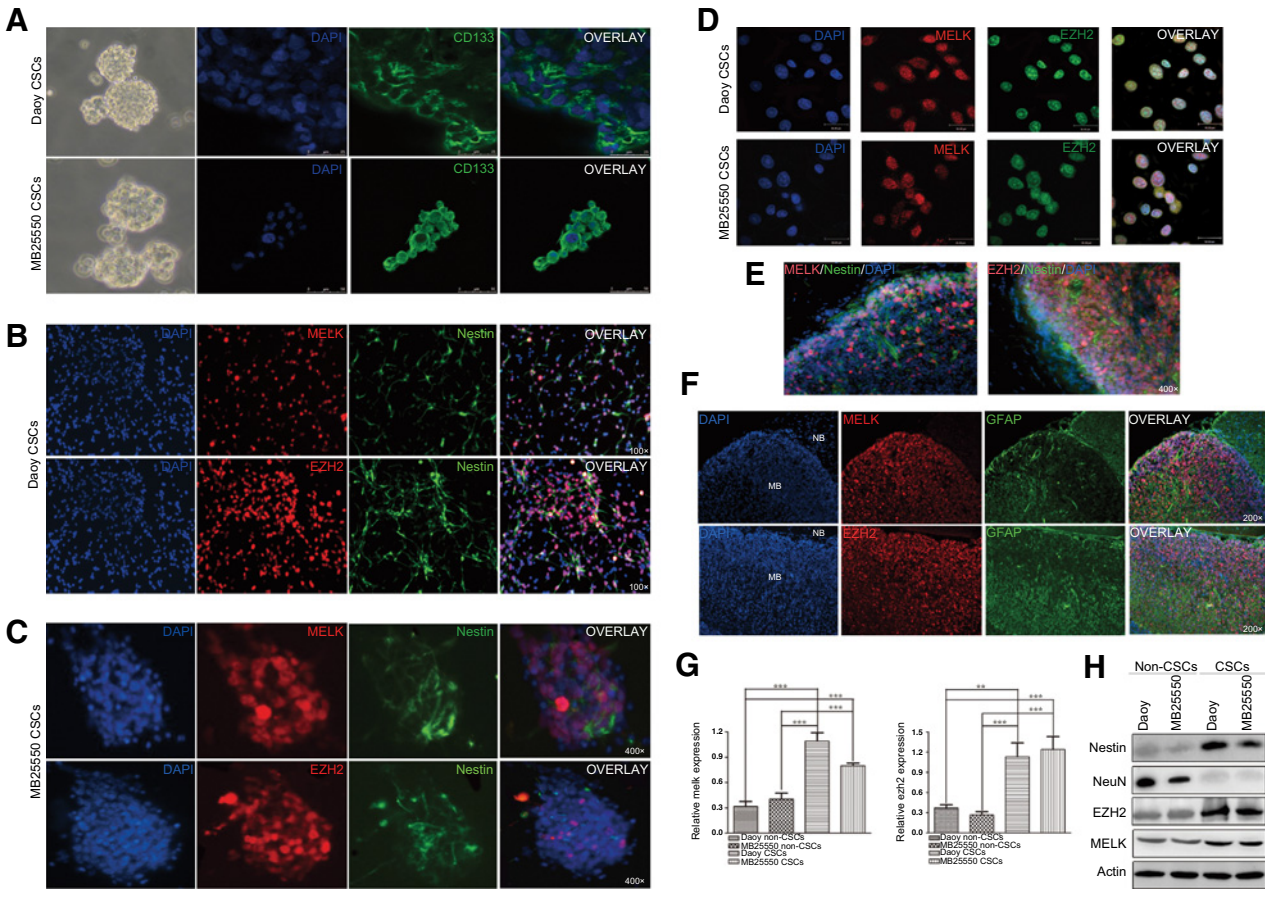

Figure 2.

MELK and EZH2 protein colocated in MBSCs. **A,** Morphology of Daoy and MB25550 CSCs spheres was shown and both were stained with CD133. Scale bar, 250 μm. **B,** Dissociated Daoy CSC-binding dishes were stained with MELK, EZH2, and Nestin showing that MELK or EZH2 was coexpressed with Nestin (100×). **C,** Immunocytochemistry of single MB25550 CSCs sphere showed that MELK or EZH2 was coexpressed with Nestin (400×). **D,** Positively stained single cells showed that MELK and EZH2 colocated in the nuclei. Scale bar, 5 μm. **E,** Immunostaining for MELK, EZH2, and Nestin in tumor tissues of $Ptc^{+/-}$ mouse model showed that MELK and EZH2 highly expressed in tumor lesions and Nestin levels also increased (400×). **F,** Immunostaining for MELK, EZH2, and GFAP in cerebellar sections of $Ptc^{+/-}$ mouse model at 12 weeks showed the positive staining of MELK, EZH2, and GFAP in tumor lesions but not in normal (200×). **G,** qRT-PCR analysis displayed that *melk* and *ezh2* mRNA expression in MBSCs was higher than that in non-MBSCs. GAPDH was used as the internal control ($P < 0.01$, $P < 0.0001$) **H,** Western blot analysis showed that the expression of MELK, EZH2, and Nestin is higher in MBSC spheres compared with the differentiated progeny (non-MBSCs), whereas NeuN expressed higher in non-MBSCs. Actin was used as the internal control.

Interaction between MELK and EZH2 occurred in MBSCs

According to the relevance of colocation, the interaction between MELK and EZH2 in MBSCs consecutively attracted more attention. First, in spite of the functions of MELK and EZH2 about development and self-renewal in NSCs, the levels presented lower than that in CSCs (Fig. 3A). Then, we examined whether MELK physically bound to EZH2 by coimmunoprecipitation (Co-IP). Endogenously expressed MELK protein in Daoy and MB25550 CSCs was pulled down by the MELK antibody, and immunoblotting analysis with EZH2 antibody was conducted, indicating that endogenous EZH2 corresponded to MELK (Fig. 3B). Similarly, binding of endogenous MELK to EZH2 was also confirmed by Co-IP of the lysates from MBSCs with EZH2 antibody (Fig. 3B). It was notable that similar results were not obtained in the differentiated tumor cells (Fig. 3B). These data suggested that the interaction between two proteins might keep cancerous stem features. Because MELK held the property of kinase, and EZH2 could methylate the specific histone proteins, it was supposed that phosphorylation and methylation might occur in the MELK–EZH2 complex. Then, we immunoblotted the pattern of phosphorylated EZH2 (p-EZH2) after the protein complex was pulled down by MELK antibody, indicating that EZH2 phosphorylation depended on MELK activity (Fig. 3C, left). Similarly, the methylated MELK status could also be detected by immunoblotting analysis after Co-IP of the lysates with EZH2 antibody, which suggested that EZH2 resulted in MELK methylation (Fig. 3C, right).

To investigate the roles of MELK and EZH2 in interacting course, Western blot analysis showed a strong suppressing levels of MELK and EZH2 in MBSCs through plasmid-mediated transfected techniques to verify knockdown efficiency (Fig. 3D). Decreased levels of p-EZH2 were observed in siMELK-expressing MBSCs compared with the nontarget control (Fig. 3E), and MKEL methylation dropped dramatically in EZH2-deficient MBSCs (Fig. 3F). EZH2 was the catalytic subunit of PRC2, which could trimethylate the Lys^{27} of H3 histone (H3K27me3), and p-EZH2

Published OnlineFirst May 23, 2017; DOI: 10.1158/1541-7786.MCR-17-0105

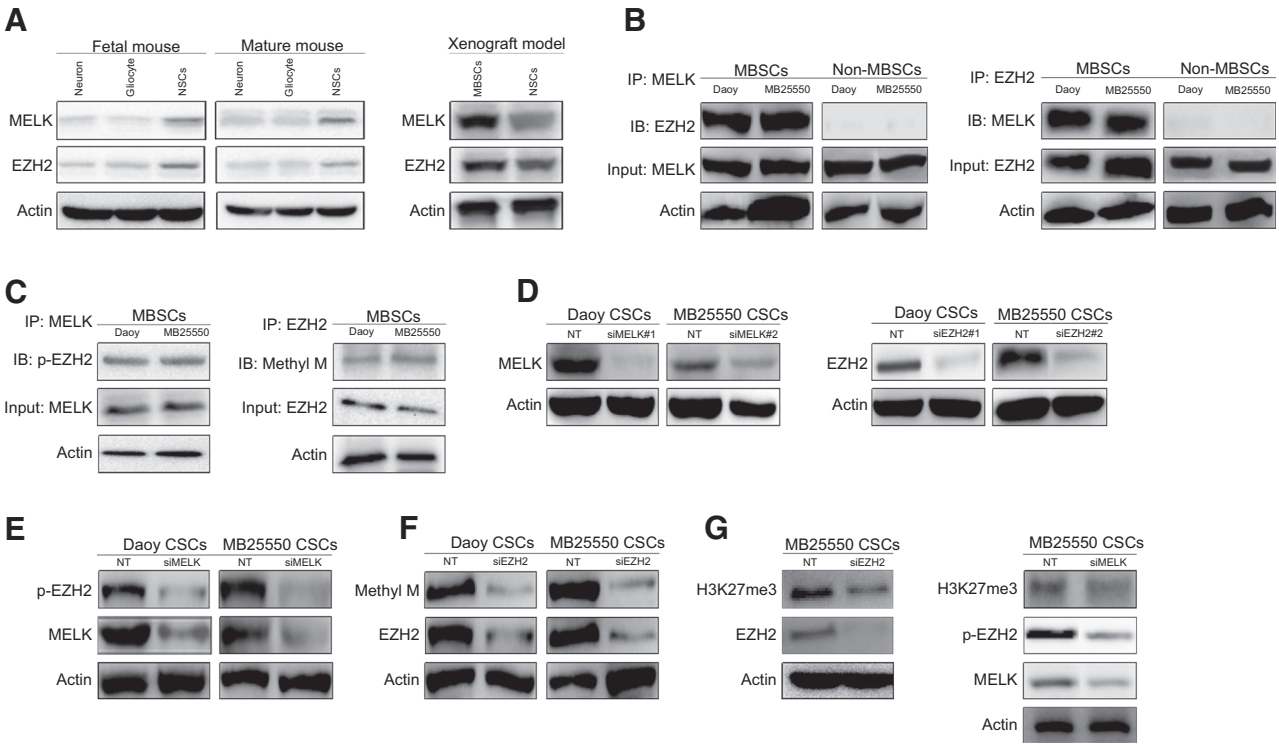

Figure 3.

Interaction between MELK and EZH2 occurred in MBSCs. **A,** Immunoblotting analysis showed that the expression of MELK and EZH2 was higher in MBSC spheres compared with the NSCs, and no expression could be checked in fetal or mature neurons and gliocytes. **B,** Left, immunoblotting analysis following Co-IP with MELK antibody showed that endogenous MELK could bind to EZH2 in both Daoy and MB25550 CSCs, but not in the non-CSCs; right, Western blot analysis following Co-IP with EZH2 antibody showed that the binding of endogenous EZH2 to MELK in both Daoy and MB25550 CSCs, but not in the non-CSCs. **C,** Immunoblotting analysis after Co-IP of the lysates with EZH2 antibody showed that MELK was methylated and vice versa; EZH2 was phosphorylated by MELK. **D,** Western blot analysis showed the elimination of MELK and EZH2 by siMELK and siEZH2 in comparison with nontarget siRNA. **E,** Immunoblotting for p-KMT6/EZH2 in siMELK-transfected Daoy and MB25550 CSCs showed that the level of p-EZH2 was attenuated due to the MELK knockdown. NT was the control for MELK knockdown. **F,** Immunoblotting for methylated MELK in siEZH2-transfected Daoy and MB25550 CSCs showed that the MELK methylation level was decreased by EZH2 knockdown. NT was the control for EZH2 knockdown. **G,** Left, EZH2 knockdown markedly decreased the staining level of H3K27me3; right, MELK knockdown not only diminished the phosphorylation of EZH2, but also reduced the methylation of H3K27me. Actin was used as the internal control.

could activate the downstream signaling pathways to promote the tumorigenicity of CSCs (36, 43). It prompted us to test the methyltransferase activity of p-EZH2. EZH2 knockdown significantly decreased H3K27 methylation similar to the insufficient MELK methylation after MBSCs were transfected with siEZH2 (Fig. 3G, left). Furthermore, the levels of H3K27me3 dropped in parallel with the phosphorylation of EZH2 due to MELK knockdown, indicating that phosphorylated condition was required for EZH2-mediated methylation (Fig. 3G, right). Thus, the above-mentioned data supported the molecular mechanism involving the interaction between MELK and EZH2 with the cancer stemness dependency.

MELK and EZH2 silencing attenuated MBSC proliferation

To extend the research achievements, we next investigated the MBSCs self-renewal *in vitro* and *in vivo* through a couple of loss-of-function studies to show the functional relevance of MELK and EZH2 in tumorigenicity. We used the neurosphere and colony formation assay as an estimation for MBSC self-proliferation. Dramatic differences were evident when MELK and EZH2 were silenced by RNAi technique (Fig. 4A). MELK and EZH2 depletion also significantly abrogated the mobility of tumor cells differentiated from the MBSCs transfected with plasmid carrying siMELK or siEZH2, which was reflected by the decreased ratio of migrating cells (Fig. 4B).

Dissociated Daoy and MB25550 CSCs infected with lentivirus encoding shMELK, shEZH2, or scramble RNA were subcutaneously injected into nude mice, respectively (Supplementary Fig. S4). Four weeks after transplantation, MBSCs expressing nontarget RNA gave rise to much larger tumor masses than MBSCs expressing shMELK and shEZH2 (Fig. 4C). Similar results were obtained after the indicated MB25550 CSCs were intracranially transplanted into nude mice. Representative microMRI scans for 3 distinct mice on the 28th day showed that significantly decreased tumor volumes existed in nude mice bearing MELK- and EZH2-deficient MB25550 CSCs compared with the faster tumor growth in control (Fig. 4D). Uptake of ^{18}F-FDG on PET/CT scans for the same 3 mice on the 28th day showed that the most extensive metastasis was observed in control, while MELK and EZH2 silencing significantly inhibited metastasis. Then, statistical graphs of standard uptake value ratio showed the more obvious potency of MELK and EZH2 knockdown (Fig. 4D). Finally, all the nude mice in control group died within about 5 weeks, whereas the median survival of animals bearing xenografts derived from

Published OnlineFirst May 23, 2017; DOI: 10.1158/1541-7786.MCR-17-0105

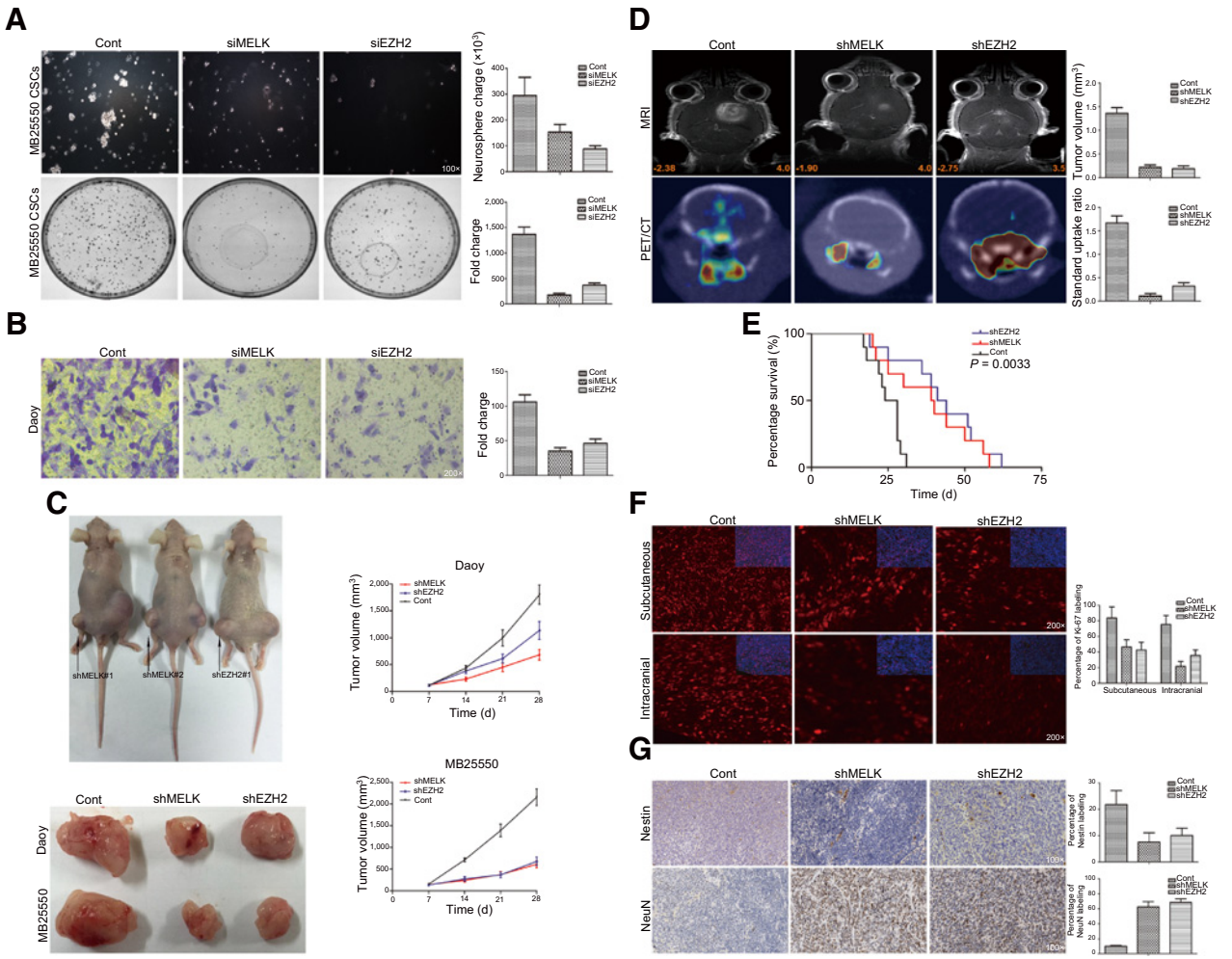

Figure 4.

MELK or EZH2 knockdown attenuated MBSCs proliferation. **A,** MELK and EZH2 knockdown had significant inhibitory effects on the neurosphere and colony formation in MB25550 CSCs (100×, 10×). The statistical graphs showed that siMELK and siEZH2 decreased the proliferation in comparison with the control ($P < 0.05$, $P < 0.05$). **B,** Cell migration was evaluated by the transwell chamber assay without coated Matrigel displaying that differentiated Daoy cells transfected with plasmid carrying siMELK or siEZH2 had defective mobility. The statistical graph showed the suppressed effects of siMELK and siEZH2 on migration compared with the control ($P < 0.05$). **C,** Daoy and MB25550 CSCs infected with lentiviral vector carrying shMELK (#1 and #2) or shEZH2#1 were subcutaneously transplanted into nude mice, respectively, and representative panels were shown as the inhibitory effects on tumor growth. Tumor volume curves were shown ($P < 0.05$, $P < 0.01$). **D,** MicroMRI scans (top) for 3 distinct nude mice with intracranial tumors derived from stereotactic xenograft of MB25550 CSCs infected with lentiviral vector carrying shMELK#1 or shEZH2#1 on 28th day showed that MELK or EZH2 knockdown attenuated tumor growth. PET/CT (lower) on 28th day demonstrated the inhibitory effects on metastasis. The graphs indicated the statistically evident difference of tumor volumes and radioactive absorption. Nontarget shRNA was used as the control ($P < 0.0001$, $P < 0.0001$). **E,** Kaplan–Meier analysis indicated that mice bearing shMELK and shEZH2-infected MB25550 CSC-derived intracranial tumors had a longer survival than the nontarget control ($P = 0.0033$). **F,** Immunostaining for Ki-67 in shMELK- and shEZH2-transfected MB25550 CSC-derived tumor sections displayed the elimination of proliferation by MELK or EZH2 knockdown compared with the nontarget control (100×). The statistical graph showed the number of cells with Ki-67–positive staining ($P < 0.05$). **G,** Representative IHC images of Nestin and NeuN staining in intracranial xenograft samples derived from nontarget shRNA, shMELK, and shEZH2 MB25550 CSCs showed the low expression of Nestin and overexpression of NeuN. Histograms represented the positive Nestin or NeuN in the specimens ($P < 0.0001$, $P < 0.0001$).

MELK- and EZH2-deficient CSCs was prolonged to 45 days (Fig. 4E). The majority of medulloblastoma cells infected with nontarget shRNA presented high proliferation, whereas only a fraction of MELK- or EZH2-deficient tumor cells were positive for Ki-67, as shown in the results of Ki-67 staining in xenograft slices (Fig. 4F). The MELK or EZH2 shRNA-transduced tumors displayed no noticeable expression of the cancer stem-like marker Nestin, but a remarkable increase of the differentiated neuron marker NeuN. In contrast, immunostaining analysis of the control tumors showed elevated percentage of Nestin and decreased level of NeuN labeling (Fig. 4G). Thereby, these data suggested that MELK and EZH2 were essential for the proliferation of medulloblastoma.

MELK or EZH2 inhibitor suppressed medulloblastoma growth

Our abovementioned statements figured out the contribution of interaction between MELK and EZH2 to medulloblastoma growth based on the elevated expression in MBSC population.

Published OnlineFirst May 23, 2017; DOI: 10.1158/1541-7786.MCR-17-0105

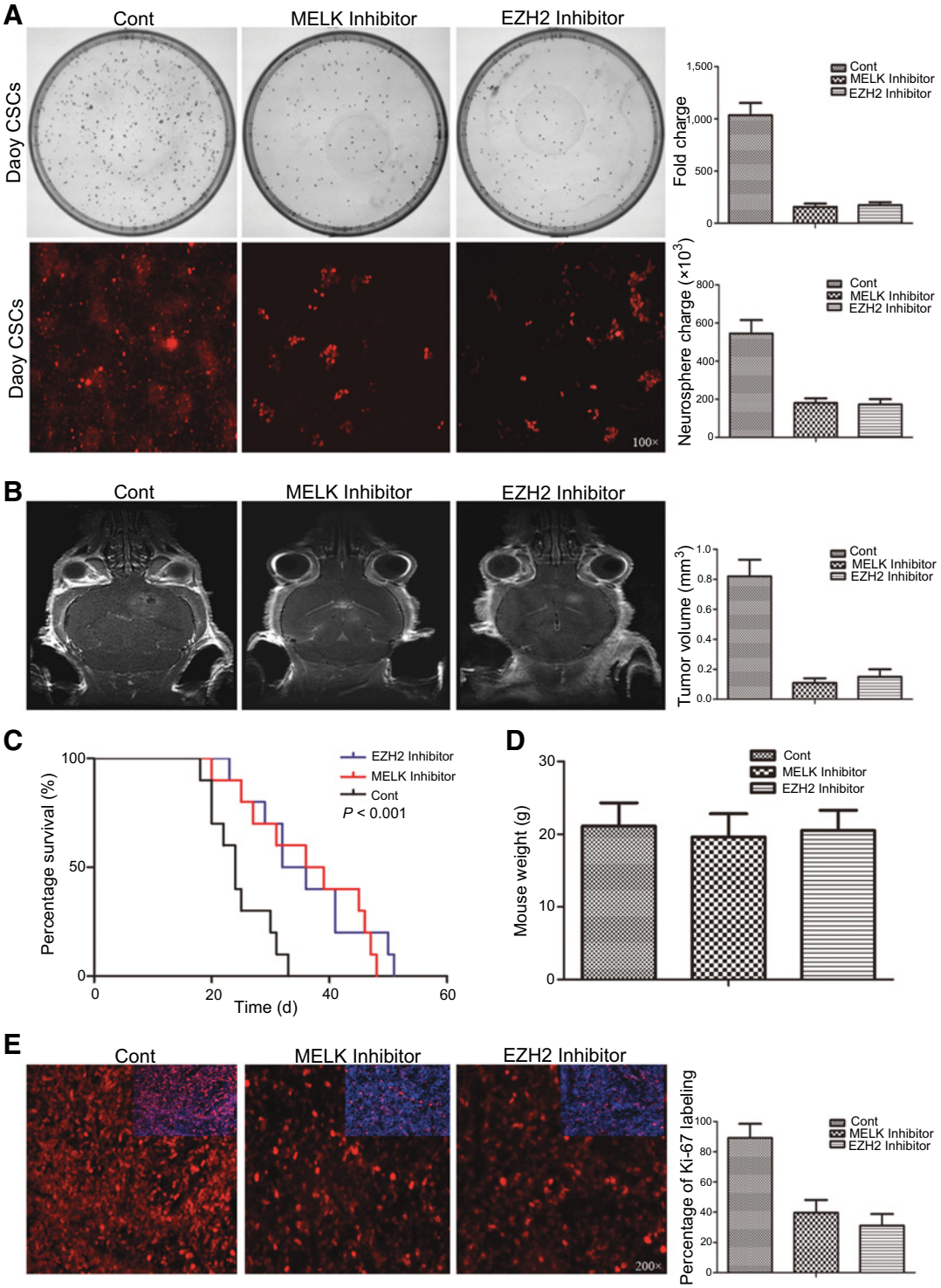

Figure 5.

MELK or EZH2 inhibitor suppressed medulloblastoma. **A,** Colony formation and neurosphere formation assay of Daoy CSCs were performed in the presence of OTSSP167, DZNep and PBS for 2 hours, and the staining with crystal violet and Ki-67 antibody displayed the roles of OTSSP167 and DZNep on the proliferation (10×, 100×). The statistical graphs showed that OTSSP167 and DZNep decreased the proliferation compared with the control ($P < 0.001$, $P < 0.01$). **B,** MicroMRI scans for 3 individual nude mice with intracranial tumors derived from MB25550 CSCs showed that OTSSP167 and DZNep markedly inhibited tumor growth compared with the control. Tumor volumes were shown in the statistical graph ($P < 0.05$). **C,** Kaplan–Meier curve demonstrated that the survival of mice bearing intracranial tumors derived from MB25550 CSCs after treatment of OTSSP167 and DZNep was better than the control ($P < 0.001$). **D,** The statistical graph of mouse weight showed that no difference existed in therapeutic and control group ($P = 0.42$). **E,** Immunostaining for Ki-67 in OTSSP167 and DZNep-treated xenografts showed the reductive proliferation after using the targeted inhibitors (100×). The graph indicated the statistically significant difference of the Ki-67–positive staining cells ($P < 0.01$).

Published OnlineFirst May 23, 2017; DOI: 10.1158/1541-7786.MCR-17-0105

We next asked whether medulloblastoma growth could be suppressed with the treatment of MELK and EZH2 inhibitors. Anchorage-dependent colony formation assay was performed to show OTSSP167 and DZNep could produce more colony reductive effects on the anchorage Daoy CSCs compared with the PBS control (Fig. 5A). Similar results were obtained in the MBSC sphere formation assay by immunostaining of Ki-67 (Fig. 5A). Interestingly, MTT data presented that no significant differences existed between the single-medication group and the combination-medication group (Supplementary Fig. S5).

We then generated cohorts of MB25550 CSCs -bearing mice to further assess whether tumor would be attenuated by targeting MELK and EZH2. According to the microMRI scans at week 4, mice treated with OTSSP167 and DZNep revealed powerful inhibition on tumor growth in contrast to the control group (Fig. 5B). The mice in MELK and EZH2 inhibitory group showed more survival benefit, with 1 of 5 mice achieving long-term survival ($\geq$50 days after transplantation, Fig. 5C). The mice weights were measured at week 6, with no differences existing in three groups, indicating that OTSSP167 and DZNep would not produce serious adverse actions (Fig. 5D). Dramatic differences were distinctive when the xenografts were immunostained for Ki-67 (Fig. 5E). Overall, these results further confirmed the functions of MELK and EZH2 activity.

Discussion

Although multiple researches have illuminated the molecular mechanisms underlying tumor initiation and progression, it still requires profound understanding of the cellular and molecular basis of medulloblastoma to identify the specific principles responsible for neoplastic proliferation. Recently, the similarity in regulating self-renewal of normal stem cells and cancer cells and the possibility in the origin of cancer cells from normal stem cells provide new insights into the conception that tumor contains "cancer stem-like cells", which present the indefinite proliferative potential contributing to the tumor growth or therapeutic resistance (7). Our previous work showed that GSCs depended on MELK/c-JUN signaling pathway to maintain survival and immature state (18). These current data present the novelty that the interaction between MELK and EZH2 occurring in MBSCs, but not in NSCs, can lead to the enhancement in proliferation and maintenance in stemness.

In this study, we report a number of findings referred to mechanisms and clinical events: (i) MELK and EZH2 proteins colocated in MBSCs are elevated in medulloblastoma and their differential expression exists in histologic subgroups; (ii) only the MBSCs, but not the NSCs, keep the extensively high levels of MELK and EZH2 to go on forming tumors; (iii) MELK can induce EZH2 phosphorylation, which is required for EZH2-mediated methylation; (iv) MELK and EZH2 play an important role in modulating stem-like cell population proliferation in pathologic process; (v) MELK and EZH2 are required for immature maintenance, and deletion of them markedly promotes differentiation; (vi) MELK and EZH2 exhibit promising values as prognostic indicators or therapeutic targets.

Elucidating the interaction between MELK and EZH2 in MBSCs is essential for understanding the roles of the two proteins in medulloblastoma proliferation. The direct interaction contributes to keep the stemness of medulloblastoma, as evidenced by the Co-IP results demonstrating that the MBSC-specific MELK binding to EZH2 differed from that in non-MBSCs (Fig. 2B). It has been reported that phosphorylation of EZH2 can enhance the STAT3 activity by mediating methylation of STAT3, which preferentially occurred in GSCs relative to non–stem-like tumor cells (36). Our data provide the following evidences that (i) MELK phosphorylates EZH2 and EZH2 methylates MELK by indefinite direct or indirect binding in MBSCs but not in non-CSCs; (ii) MELK and EZH2 colocate with Nestin in SHH-MB mouse model sections, which sheds light on the function of MELK–EZH2 pathway in regulating the MBSCs self-renewal. Likewise, given the exaggerated profiles of MELK and EZH2 in a high level of Ki-67$^+$–associated medulloblastoma samples, such as the large-cell/anaplastic or SHH subgroup (Fig. 1A and C; Supplementary Fig. S3A), it also highlights the impacts of the two in tumor growth. Furthermore, MELK silencing inhibits EZH2 phosphorylation and EZH2 depletion also represses MELK methylation, thereby blocking medulloblastoma proliferation *in vitro* and *in vivo*. However, we cannot rule out whether the interaction regulates medulloblastoma proliferation in the same molecular basis as previously identified in GBM (18, 35), which demands further research.

Our data reveal that different expression levels of MELK and EZH2 exist between MBSCs and NSCs. In addition, the two protein expressions are rarely found in normal differential neurons and gliocytes (Figs. 1A and 3A). In this study, the usage of CD133 to mark MBSCs has its specific drawbacks as follows: on one hand, the percentage of CD133$^+$ cells is less than that of CD15$^+$ in medulloblastoma, which shows greater potential in labeling the CSCs (44). On the other hand, only one marker is chosen to identify MBSCs with more meaningful results probably coming from two indexes, such as CD133+CD15, CD133+CD34, or CD133+nestin. However, stem cell microenvironment has changed a great deal with the initiation and progression of neoplasms. Studies have suggested the vital role of tumor microenvironments that normally operate to regulate various types of protein stabilities during CSCs self-proliferation (45). CSCs are "clever" enough to modify the microenvironment by recruiting agents to make others, including vessels, astrocytes, fibroblasts, etc., serve themselves with the goal of maintaining self-renewal (46). For example, in medulloblastoma, GFAP$^+$ staining represents that a few astrocytes in tumor microenvironment are activated in human and mouse model tissues (Fig. 2F; Supplementary Fig. S3B), and this population of cells may secrete various factors, such as sonic hedgehog, TGFβ, CCL2, etc., to support MBSC self-renewal and achieve malignancy (47).

Recent discoveries have demonstrated four distinctive molecular subtypes of human medulloblastoma: SHH, WNT, Group 3, and Group 4 (3). In our research, the Daoy cell line and *Ptc*$^{+/-}$ mouse model are classified as the SHH subgroup, and MB25550 cells are also derived from the SHH-MB (Supplementary Fig. S6A; refs. 48, 49). MELK interacts with EZH2 in Daoy and MB25550 CSCs, and the xenografts that develop from the two kinds of MBSCs are strongly attenuated by RNA knockdown or inhibitors. Initial findings have revealed Nestin-bound hedgehog pathway to promote the development of SHH-MB (45). The sample of SHH-MB in this research also displays the high expression of Nestin (Supplementary Fig. S6B). Our current work shows that loss of MELK or EZH2 dramatically inhibits Nestin expression, suggesting that targeting the interaction between two proteins may present a promising therapeutic strategy for the treatment of SHH-MB. Further research is warranted to investigate the

Published OnlineFirst May 23, 2017; DOI: 10.1158/1541-7786.MCR-17-0105

mechanisms and functions of the interaction between MELK and EZH2 in other three subgroups.

The observation of proliferative regulation by interaction between MELK and EZH2 has made it an attractive target candidate for diagnosis and treatment of medulloblastoma. On one hand, MELK and EZH2 expression are examined by IHC in 88 human medulloblastoma samples, and the correlation with prognosis is assessed by Kaplan–Meier, Cox proportional model, and logistic analysis, showing that MELK and EZH2 are strongly linked to the prognosis of patients with medulloblastoma, despite the negative result of EZH2 in Kaplan–Meier analysis, which needs more samples to be evaluated (Fig. 1E and F; Tables 1 and 2). On the other hand, the impact of MELK and EZH2 knockdown or inhibition on tumor growth in our work would facilitate the management strategies of MELK or EZH2 inhibitors in medulloblastoma patients, which is in agreement with the previous significant data on targeting EZH2 in medulloblastoma (50). However, combination of the two drugs does not exhibit the indicated advance and the reasons may be that both the inhibitors focus on only the same MELK/EZH2 pathway. Then, the research involved in the effects of MELK or EZH2 inhibitor with other first-line antineoplastics (methotrexate, cisplatin, etc.) on medulloblastoma will be required in the future program. Besides, in many cases, tumor exhibits relapse or resistance to chemo- and radiotherapy due to the population of CSCs. Given that MELK or EZH2 silencing significantly reduces the Nestin expression and augments the NeuN expression to break the medulloblastoma stemness and promote the differentiation (Fig. 4G), it is possible that lowering the malignancy and elevating the sensitivity to therapies can rely on the modulation of the two oncogenic proteins.

On the basis of our studies, it is the first novel evidence that the phosphorylation and methylation between MELK and EZH2 occurring in MBSCs, but not in NSCs, can regulate the proliferation and differentiation of medulloblastoma. Meanwhile, MELK immunostaining presents the prognostic value for medulloblastoma patients. Through the loss-of-function study, MELK and EZH2 silencing or inhibition suppresses the neurosphere formation and attenuates the MBSC-derived xenograft growth, and also induces the differentiation of MBSCs. In conclusion, further research in considering MELK and EZH2 as prognosis indicators and/or therapeutic targets may contribute to improving diagnosis and treatment of patients with medulloblastoma. Potentially, this strategy also can be expanded to other cancers if the interaction between MELK and EZH2 functions in a similar way to regulate the tumorigenicity.

Disclosure of Potential Conflicts of Interest

No potential conflicts of interest were disclosed.

Authors' Contributions

Conception and design: H. Liu, C. Gu
Development of methodology: H. Liu, Q. Sun
Acquisition of data (provided animals, acquired and managed patients, provided facilities, etc.): H. Liu, Y. Sun, H. Yuan, X. Qi, H. Wang, M. Zhang, H. Zhang
Analysis and interpretation of data (e.g., statistical analysis, biostatistics, computational analysis): H. Liu, S. Pang
Writing, review, and/or revision of the manuscript: H. Liu, C. Gu
Administrative, technical, or material support (i.e., reporting or organizing data, constructing databases): J. Zhang, C. Yu, C. Gu
Study supervision: Q. Sun, C. Yu, C. Gu

Acknowledgments

The authors acknowledge Yanan Wang, MD, PhD, Chinese Academy of Medical Sciences and Peking Union Medical College, Beijing, P.R. China, for the Daoy cell line and $Ptc^{+/-}$ mouse model tumor sections, as well as Ichiro Nakano, MD, PhD, in Department of Neurological Surgery of The Ohio State University (Columbus, OH) for the plasmids encoding shMELK and scramble RNA.

Grant Support

This work was supported by the Scientific Research Common Program of Beijing Commission of Education grant KM201610025027 (to C.Y. Gu), Beijing Municipal Science & Technology Commission grant Z151100004015165 (to M.S. Zhang), and National Nature Science Foundation of China81372694 (to C.J. Yu).

The costs of publication of this article were defrayed in part by the payment of page charges. This article must therefore be hereby marked *advertisement* in accordance with 18 U.S.C. Section 1734 solely to indicate this fact.

Received February 23, 2017; revised April 11, 2017; accepted May 18, 2017; published OnlineFirst May 23, 2017.

References

1. Northcott PA, Jones DT, Kool M, Robinson GW, Gilbertson RJ, Cho YJ, et al. Medulloblastomics: the end of the beginning. Nat Rev Cancer 2012;12:818–34.
2. Gibson P, Tong Y, Robinson G, Thompson MC, Currle DS, Eden C, et al. Subtypes of medulloblastoma have distinct developmental origins. Nature 2010;12:1095–99.
3. Louis DN, Perry A, Reifenberger G, von Deimling A, Figarella-Branger D, Cavenee WK, et al. The 2016 World Health Organization classification of tumors of the central nervous system: a summary. Acta Neuropathol 2016;113:803–20.
4. Smoll NR. Relative survival of childhood and adult medulloblastomas and primitive neuroectodermal tumors (PNET). Cancer 2012;118:1313–22.
5. Thompson EM, Hielscher T, Bouffet E, Remke M, Luu B, Gururangan S, et al. Prognostic value of medulloblastoma extent of resection after accounting for molecular subgroup: a retrospective integrated clinical and molecular analysis. Lancet Oncol 2016;17:484–95.
6. Ramaswamy V, Remke M, Bouffet E, Faria CC, Perreault S, Cho YJ, et al. Recurrence patterns across medulloblastoma subgroups: an integrated clinical and molecular analysis. Lancet Oncol 2013;14:1200–07.
7. Reya T, Morrison SJ, Clarke MF, Weissman IL. Stem cells, cancer and cancer stem cells. Nature 2001;414:105–111.
8. Holland EC, Celestino J, Dai C, Schaefer L, Sawaya RE, Fuller GN. Combined activation of Ras and Akt in neural progenitor induces glioblastoma formation in mice. Nat Genet 2000;25:55–57.
9. Fan X, Eberhart CG. Medulloblastoma stem cells. J Clin Oncol 2008;26:2821–27.
10. Hemmati HD, Nakano I, Lazareff JA, Masterman-Smith M, Geschwind DH, Bronner-Fraser M, et al. Cancerous stem cells can arise from pediatric brain tumors. Proc Natl Acad Sci 2003;100:15178–83.
11. Gli M, Yang Y, Lee Y, Choi I, Ha H. Cloning and expression of a cDNA encoding a novel protein serine/threonine kinase predominantly expressed in hematopoietic cells. Gene 1997;195:295–301.
12. LaPak KM, Burd CE. The molecular balancing act of p16(INK4a) in cancer and aging. Mol Cancer Res 2014;12:167–83.
13. Pickard MR, Green AR, Ellis IO, Caldas C, Hedge VL, Mourtada-Maarabouni M, et al. Dysregulated expression of Fau and MELK is associated with poor progression in breast cancer. Breast Cancer Res 2009;11:R60.
14. Nakano I, Masterman-Smith M, Saigusa K, Paucar AA, Horvath S, Shoemaker L, et al. Maternal embryonic leucine-zipper kinase is a key regulator

Published OnlineFirst May 23, 2017; DOI: 10.1158/1541-7786.MCR-17-0105

of the proliferation of malignant brain tumors, including brain tumor stem cells. J Neurosci Res 2008;86:48–60.
15. Saito R, Nakauchi H, Watanabe S. Serine/threonine kinase, Melk, regulates proliferation and glial differentiation of retinal progenitor cells. Cancer Sci 2012;103:42–49.
16. Xia H, Kong SN, Chen J, Shi M, Sekar K, Seshachalam VP, et al. MELK is an oncogenic kinase essential for early hepatocellular carcinoma recurrence. Cancer Lett 2016;383:85–93.
17. Inoue H, Kato T, Oluqbile S, Tamura K, Chung S, Miyamoto T, et al. Effective growth-suppressive activity of maternal embryonic leucine-zipper kinase (MELK) inhibitor against small cell lung cancer. Oncotarget 2016;7:13621–33.
18. Gu CY, Banasavadi-Siddegowda YK, Joshi K, Nakamura Y, Kurt H, Gupta S, et al. Tumor-specific activation of the C-JUN/MEILK pathway regulates glioma stem cell growth in a p53-dependent manner. Stem Cells 2013;31:870–81.
19. Marie SK, Okamoto OK, Uno M, Hasegawa AP, Oba-Shinjo SM, Cohen T, et al. Maternal embryonic leucine zipper kinase transcript abundance correlates with malignancy grade in human astrocytomas. Int J Cancer 2008;122:807–15.
20. Li YH, Wang Z, Shi H, Li H, Li L, Fang R, et al. HBXIP and LSD1 scaffolded by lncRNA Hotail mediate transcriptional activation by c-Myc. Cancer Res 2016;76:293–304.
21. Aloia L, Di Stefano B, Di Croce L. Polycomb complexes in stem cells and embryonic development. Development 2013;140:2525–34.
22. Laible G, Wolf A, Dorn R, Reuter G, Nislow C, Lebersorger A, et al. Mammalian homologues of the Polycomb-group gene Enhancer of zeste mediate gene silencing in *Drosophila* heterochromatin and at S. cerevisiae telomeres. EMBO J 1997;16:3219–32.
23. Margueron R, Reinberg D. The Polycomb complex PRC2 and its mark in life. Nature 2011;469:343–49.
24. Ringrose L, Paro R. Epigenetic regulation of cellular memory by the Polycomb and Trithorax group proteins. Annu Rev Genet 2004;38:413–43.
25. Tonini T, Bagella L, D'Andrilli G, Claudio PP, Giordano A. Ezh2 reduces the ability of HDAC1-dependent pRb2/p130 transcriptional repression of cyclin A. Oncogene 2004;23:4930–37.
26. Chen H, Tu SW, Hsieh JT. Down-regulation of human DAB2IP gene expression mediated by polycomb Ezh2 complex and histone deacelyase in prostate cancer. J Biol Chem 2005;280:22437–44.
27. Su IH, Dobenecker MW, Dickinson E, Oser M, Basavaraj A, Marqueron R, et al. Polycomb group protein ezh2 controls actin polymerization and cell signaling. Cell 2005;121:425–36.
28. Huether R, Dong L, Chen X, Wu G, Parker M, Wei L, et al. The landscape of somatic mutations in epigenetic regulators across 1,000 paediatric cancer genomes. Nat Commun 2014;5:3630–37.
29. Smits M, van Rijn S, Hulleman E, Biesmans D, van Vuurden DG, Kool M, et al. EZH2-regulated DAB2IP is a medulloblastoma tumor suppressor and a positive marker for survival. Clin Cancer Res 2012;18:4048–58.
30. Scott MT, Korfi K, Saffrey P, Hopcroft LE, Kinstrie R, Pellicano F, et al. Epigenetic reprogramming sensitizes CML stem cells to combined EZH2 and tyrosine kinase inhibition. Cancer Discov 2016;6:1248–57.
31. Adamik J, Jin S, Sun Q, Zhang P, Weiss KR, Anderson JL, et al. EZH2 or HDAC1 inhibition reverses multiple myeloma-induced epigenetic suppression of osteoblast differentiation. Mol Cancer Res 2017;15:405–17.
32. Dardenne E, Beltran H, Benelli M, Gayvert K, Berger A, Puca L, et al. N-Myc induces an EZH2-mediated transcriptional program driving neuroendocrine prostate cancer. Cancer Cell 2016;30:563–77.
33. Suva ML, Riggi N, Janiszewska M, Radovanovic I, Provero P, Stehle JC, et al. EZH2 is essential for glioblastoma cancer stem cell maintenance. Cancer Res 2009;69:9211–18.
34. Dubuc AM, Remke M, Korshunov A, Northcott PA, Zhan SH, Mendez-Lago M, et al. Aberrant patterns of H3K4 and H3K27 histone lysine methylation occur across subgroups in medulloblastoma. Acta Neuropathol 2013;125:373–84.
35. Kim SH, Joshi K, Ezhilarasan R, Myers TR, Siu J, Gu C, et al. EZH2 protects glioma stem cells from radiation-induced cell death in a MELKFOXM1-dependent manner. Stem Cell Rep 2015;4:226–38.
36. Kim E, Kim M, Woo DH, Shin Y, Shin J, Chang N, et al. Phosphorylation of EZH2 activates STAT3 signaling via STAT3 methylation and promotes tumorigenicity of glioblastoma stem-like cells. Cancer Cell 2013;23:839–52.
37. Jijiwa M, Demir H, Gupta S, Leung C, Joshi K, Orozco N, et al. CD44v6 regulates growth of brain tumor stem cells partially through the AKT-mediated pathway. PLoS One 2011;6:e24217.
38. Liu HL, Sun QW, Zhang MS, Zhang ZH, Fan XY, Yuan HY, et al. Differential expression of Folate receptor 1 in medulloblastoma and the correlation with clinicopathological characters and target therapeutic potential. Oncotarget 2017;8:23048–60.
39. Schmid RS, Simon JM, Vitucci M, McNeill RS, Bash RE, Werneke AM, et al. Core pathway mutation induce de-differentiation of murine astrocytes into glioblastoma stem cells that are sensitive to radiation but resistant to temozolomide. Neuro Oncol 2016;18:962–73.
40. Chung S, Suzuki H, Miyamoto T, Takamatsu N, Tatsuguchi A, Ueda K, et al. Development of an orally-administrative MELK-targeting inhibitor that suppresses the growth of various types of human cancer. Oncotarget 2012;3:1629–40.
41. Gao SB, Zheng QF, Xu B, Pan CB, Li KL, Zhao Y, et al. EZH2 repress target genes through H3K27-dependent and K3K27-independent mechanisms in hepatocellular carcinoma. Mol Cancer Res 2014;12:1388–97.
42. Brennan CW, Verhaak RG, Mckenna A, Campos B, Noushmehr H, Salama SR, et al. The somatic genomic landscape of glioblastoma. Cell 2013;155:462–77.
43. Xu K, Wu ZJ, Gromer AC, He HH, Cai C, Lis RT, et al. EZH2 oncogenic activity in castration-resistant prostate cancer cells is polycomb-independent. Science 2012;338:1465–70.
44. Read TA, Fogarty MP, Markant SL, Mclendon RE, Wei Z, Ellison DW, et al. Identification of CD15 as a marker for tumor-propagating cells in a mouse model of medulloblastoma. Cancer Cell 2009;15:135–47.
45. Li P, Lee EH, Du F, Gordon RE, Yuelling LW, Liu Y, et al. Nestin mediates Hedgehog pathway tumorigenesis. Cancer Res 2016;76:5573–83.
46. Byrd T, Grossman RG, Ahmed N. Medulloblastoma-biology and microenvironment: a review. Pediatr Hematol Oncol 2012;29:495–06.
47. Smeester BA, O'Brien EE, Michlitsch KS, Lee JH, Beitz AJ. The relationship of bone-tumor-induced spinal cord astrocyte activation and aromatase expression to mechanical hyperalygesia and cold hypersensitivity in intact female and ovariectomized mice. Neuroscience 2016;324:344–54.
48. Blüml S, Margol AS, Sposto R, Kennedy RJ, Robison NJ, Vali M, et al. Molecular subgroups of medulloblastoma identification using noninvasive magnetic resonance spectroscopy. Neuro Oncol 2016;18:126–31.
49. Ivanov DP, Coyle B, Walker DA, Grabowska AM. *In vitro* models of medulloblastoma: choosing the right tool for the job. J Biotechnol 2016;236:10–25.
50. Alimova I, Venkataraman S, Harris P, Marquez VE, Northcott PA, Dubuc A, et al. Targeting the enhancer of zeste homologue 2 in medulloblastoma. Int J Cancer 2012;131:1800–09.

AACR American Association for Cancer Research

Molecular Cancer Research

MELK and EZH2 Cooperate to Regulate Medulloblastoma Cancer Stem-like Cell Proliferation and Differentiation

Hailong Liu, Qianwen Sun, Youliang Sun, et al.

Mol Cancer Res Published OnlineFirst May 23, 2017.